Journal of Power Sources 348 (2017) 212–218

Contents lists available at ScienceDirect

Journal of Power Sources

journal homepage: www.elsevier.com/locate/jpowsour

Membrane-less micro fuel cell based on two-phase flow

S.M.H. Hashemi*, M. Neuenschwander, P. Hadikhani, M.A. Modestino, D. Psaltis

École Polytechnique Fédérale de Lausanne (EPFL), Institute of Microtechnology, Laboratory of Optics, Lausanne, CH-1015, Switzerland

HIGHLIGHTS

- A microfluidic fuel cell (MFFC) with two phase streams is demonstrated.
- Two-phase flows of H_2 and O_2 gas move parallel to each other without mixing.
- Power density is one order of magnitude higher than the single-phase system.
- The results open up a pathway for revisiting the use of hydrogen fuel in MFFCs.

GRAPHICAL ABSTRACT

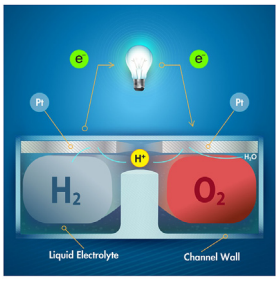

ARTICLE INFO

Article history:
Received 31 October 2016
Received in revised form
20 February 2017
Accepted 23 February 2017
Available online 7 March 2017

Keywords:
Microfluidic fuel cell (MFFC)
Membrane-less
Two-phase flow
Hydrogen
Mass transfer

ABSTRACT

Most microfluidic fuel cells use highly soluble fuels and oxidants in streams of liquid electrolytes to overcome the mass transport limitations that result from the low solubility of gaseous reactants such as hydrogen and oxygen. In this work, we address these limitations by implementing controlled two-phase flows of these gases in a set of microchannels electrolytically connected through a narrow gap. Annular flows of the gases reshape the concentration boundary layer over the surface of electrodes and increase the mass-transport limited current density in the system. Our results show that the power density of a two-phase system with hydrogen and oxygen streams is an order of magnitude higher than that of single phase system consisting of liquid electrolytes saturated with the same reactants. The reactor design described here can be employed to boost the performance of MFFCs and put them in a more competitive position compared to membrane based fuel cells.

1. Introduction

Close to two centuries have passed since the first reports of hydrogen fuel cells [1]. These interesting early power generators did not reach practical use until recently due to various technical, social, political, and economic reasons. Driven by environmental factors, hydrogen fuel cell vehicles have regained attention, and are commercially available today [2,3]. Portable electronics is another sector with high potential for fuel cells, given the possibility of achieving higher power densities than batteries. Implementation in this sector requires the development of light weight and compact fuel cells. Micro fuel cells are a class of power sources that can address these requirements [4–9]. Additionally, their compatibility with semiconductor manufacturing processes makes micro fuel cells a promising power source for consumer electronics.

An interesting group of micro fuel cells are microfluidic fuel cells (MFFCs) that allow for the implementation of laminar co-flow of an oxidant and a fuel stream parallel to each other. In this configuration, mixing can only happen through diffusion at their interface between the streams [10–14]. If the flow is fast enough, i.e. high Péclet number regime, this diffusion is negligible and does not affect the performance; even without implementing separation

* Corresponding author.
E-mail address: mohammad.hashemi@epfl.ch (S.M.H. Hashemi).

http://dx.doi.org/10.1016/j.jpowsour.2017.02.079

membranes. Developing fuel cells without membranes would reduce the cost, size and weight of the device. It can also lead to a better performance compared to conventional fuel cells as liquid electrolytes have higher ionic conductivity than solid-state ones. Despite these advantages, membrane-less devices face significant hurdles since the fuel and oxidant need to be dissolved into liquid electrolytes. Promising clean fuels such as hydrogen have very low solubility in liquid electrolytes (<0.8 mol m^{-3} at standard conditions), which introduces significant mass transport limitations and restricts the peak power density to less than 1 mW/cm^2 [15,16]. In order to address this problem, alternative chemicals with high solubility in liquid electrolytes can be implemented. Kjeang et al. demonstrated that by flowing aqueous vanadium redox species through porous electrodes, power densities as high as 131 mW/cm^2 can be achieved. The two streams pass through highly porous electrodes with numerous catalytic active sites and enter a microchannel where they flowed parallel to each other and exit the chip downstream [17]. An improved cell design has been shown to provide power densities as high as 330 mW cm^{-2} [18]. Da Mota et al. used borohydride and cerium ammonium nitrate as fuel and oxidant in a cell where the plate electrodes contained herringbone structures to induce chaotic mixing and improve mass transport. In order to prevent the fuel and oxidant crossover, they integrated a 10 μm porous separator into the device and achieved a peak power of 250 mW cm^{-2} [19]. Despite these promising demonstrations, use of high energy density and economically viable fuels such as hydrogen can potentially promote their deployment. In this study, we revisit hydrogen as a fuel and devise an approach that mitigates the mass transport limitations that has restricted the development of high power density hydrogen MFFCs. In order to go beyond the saturation limit of gases in liquid electrolytes, two-phase flows will need to be considered. Implementing two-phase flows, requires the conception of a mechanisms to introduce and maintain separate H_2 and O_2 gas streams with minimal level of mixing. Furthermore, these gaseous streams will need to be encapsulated in a continuous ionically conductive phase, i.e. liquid electrolyte. Under this configuration, gas crossover would only occur via diffusion, and as far as the stream velocity is high, mixing between the two gas streams would be negligible [20]. In the following sections, we describe a method that satisfies all of these conditions and allowed for the demonstration of a proof-of-concept device that delivers one order of magnitude higher power density compared to its single phase counterpart. Such a method can be implemented in other electrochemical systems where mass transfer is a major performance barrier.

2. Working principle

It is known that droplets and bubbles confined to microchannels adapt their morphology to minimize their surface energy. This property has been used to trap or guide these deformable entities into cavities or rails at the walls of microchannels [21–25]. Making use of this principle, two streams of H_2 and O_2 gas inside electrolyte are confined to two separated microchannels connected by a shallow ionic bridge. The elongated bubbles are surrounded by the liquid electrolyte which fills in the shallow mid channel as well. The top wall of each gas channel is covered by a thin platinum electrode where the gases can diffuse to their surface through the very thin liquid film wetting the hydrophilic channels walls. In this way, the bubbles act as reservoirs of fuel and oxidant feeding the thin liquid layer that separates the gas streams from the electrodes. Furthermore, the protons can move freely in this layer and reach the

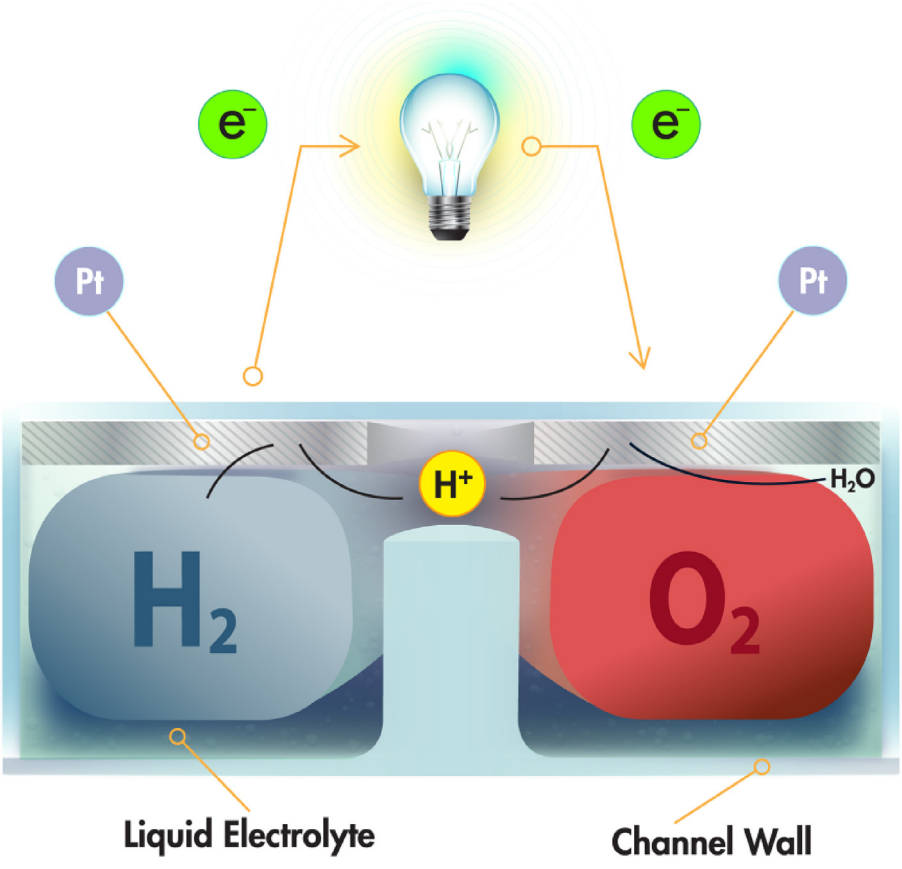

Fig. 1. Schematic representation of the two-phase flow concept in a membrane-less fuel cell.

cathode through the shallow gap. A three dimensional illustration of this structure is provided in Fig. 1. It is worth noting that a similar channel profile has been previously used in an MFFC with formic acid as fuel and potassium permanganate as oxidant in order to reduce the cross-diffusion area [26].

3. Analytical and numerical model

To gain insights into the expected mass transport enhancement from a two-phase configuration over single phase one, a simple analytical model has been developed for the former and a 3D numerical model in COMSOL for the latter. In both cases, only mass transport limitations have been taken into account, as they are expected to be the dominant source of losses at maximum current density which is dictated by the maximum mass flux of reactants towards the surface of the electrodes.

For the two-phase case, the mass transport inside the thin liquid electrolyte film is assumed to be one dimensional and diffusion dominated. Under these conditions, the mass transport of gases can be described by,

$$\frac{\partial \mathbf{c}}{\partial \mathbf{t}} = \mathbf{D}\frac{\partial^2 \mathbf{c}}{\partial \mathbf{y}^2}$$

where *c*, *t*, *D*, and y are the concentration of species, time, diffusion coefficient, and spatial coordinate in the cross flow direction, respectively. At steady state, the solution to this equation, subject to a zero concentration of reactant at the surface of the electrode (Fig. 2a), is linear and in the form of $\mathbf{c}(\mathbf{y}) = \frac{\mathbf{C_{sat}}}{\mathbf{d}}\mathbf{y}$, where *d* corresponds to the thickness of liquid film and C_{sat} to the equilibrium concentration of species at the gas/liquid interface. Assuming a uniform Fickian diffusion over the electrode's area, the average flux of species for the two-phase case can be estimated to be $\mathbf{D}\frac{\mathbf{C_{sat}}}{\mathbf{d}}$. Assuming equal average velocities for the gas and liquid phases in the annular flow (i.e. homogeneous conditions) the liquid film thickness, *d*, can be calculated (Details are provided in the supporting information (SI)). The homogeneity condition for elongated bubbles in rectangular channels has been observed before [27]. The values for D and C_{sat} for H_2 are used in the calculations since it is the transport limited reactant. In other words, the product of DC_{sat}/n for hydrogen in water at 25 °C is 1.75×10^{-9} mol m^{-1} s^{-1} versus 2.6×10^{-9} mol m^{-1} s^{-1} for oxygen, where n is the number of moles for each reactant in the overall reaction, i.e. $2H_2 + O_2 \rightarrow H_2O$.

The 3D model is developed for half of the cell subject to a zero concentration of reactant at the surface of the electrode as depicted in Fig. 2b. The problem is solved in COMSOL by coupling laminar flow and transport of dilute species modules. The average mass flux over the electrode is calculated from the results and given in Table 1 for comparison with experimental results. The general trend shows that a short circuit density enhancement between 500 and 1100% is expected depending on the flow rates used.

4. Experimental section

4.1. Device architecture and fabrication

The fluidic channels were dry etched into a double sided polished silicon wafer with one micron of wet oxide layer on both sides acting as mask for the etching process. The process involves two photolithography steps on the front side and one on the backside for fluidic ports and electrical connection holes. At the end of the process, the initial oxide layer was removed in an HF bath and a new 170 nm dry oxide layer was grown to render the surface hydrophilic and electrically insulating. There are six fluidic ports on

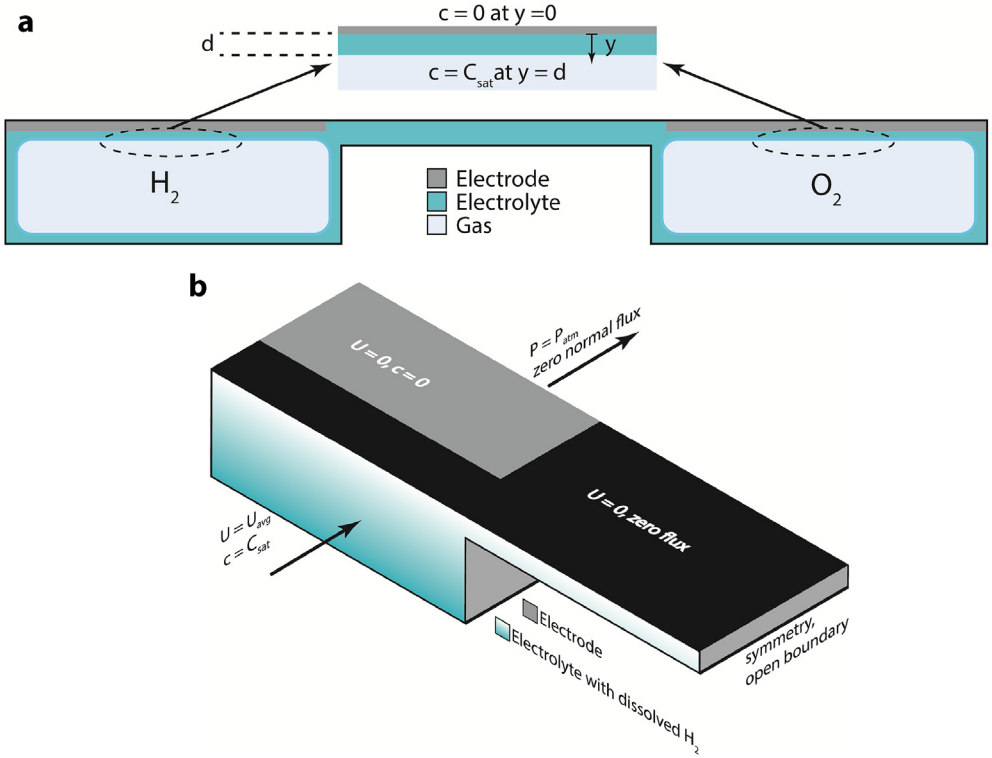

Fig. 2. a) Schematic of the cell cross section for the two-phase configuration and the boundary conditions for the diffusion equation. Approximate determination of the liquid film thickness is provided in the supporting information. b) 3D schematic of the modeled geometry with applied boundary conditions. U_{avg} is the average velocity and P_{atm} the atmospheric pressure.

the device: two for introducing the liquid electrolyte, two for gas injection, and the last two as the outlet. The 170 nm thick Pt electrodes are patterned on a Pyrex wafer using photolithography and ion beam etching. A 10 nm Ti seed layer was deposited prior to Pt sputtering to promote adhesion. The two wafers were then cleaned, aligned, and bonded anodically. The detailed procedure is shown in Fig. S1.

The widths and depths of the two deep channels are 135 and 50 μm respectively and the width and depth of the connecting gap is 130 and 10 μm, respectively. The elongated gas bubbles contained in the liquid phase are generated in an upstream cross junction before entering the main channel. The length of all channels is 1 cm out of which 5 mm are covered with the platinum electrodes and the rest are used as a transparent window for visual inspection. The layout of the fluidic channels is shown in Fig. 3a. The main channels end up into a Y shaped bifurcation separating the oxidant and fuel flows downstream. Several narrow shunt channels were introduced to balance the pressure between the two outlet channels [28]. This ensures no clogging by bubbles at the outlets as can be seen from Fig. 5 and Movie S2. The platinum electrodes are 5 mm long and 120 μm wide and the gap between the two is 160 μm. This accounts for an active electrode area over the channels of 0.006 cm^2.

There are six cells on each pair of wafers (Fig. S2) which are diced and used individually for measurements. After dicing, PDMS pieces with punched holes are bonded on top of fluidic ports to provide a flexible bed for tubing and electrical wires are soldered to the open area of Pt electrodes in order to connect the device to a potentiostat for characterization as depicted in Fig. 3b.

4.2. Experimental set-up and characterization

The two electrolyte inlets are connected to two plastic syringes from Becton Dickinson filled with 1 M sulfuric acid and mounted on a dual syringe pump (Cronus Sigma 2000). The two gas inlets are connected to two gas tight syringes from SGE Analytical Science, each filled with pure hydrogen and oxygen and mounted on a similar pump. The outlets are drained into a beaker using tubes of the same size. For the single phase measurements, the gas inlet tubes are blocked by a clipper and the electrolytes in each syringe is saturated with hydrogen and oxygen prior to the measurements by bubbling each gas through 1 M sulfuric acid solutions placed in separate containers for 15 minutes. Prior to this saturation process, the electrolyte was bubbled with N_2 to eliminate traces of O_2 from ambient air.

In the case of two-phase measurements, the operation of the

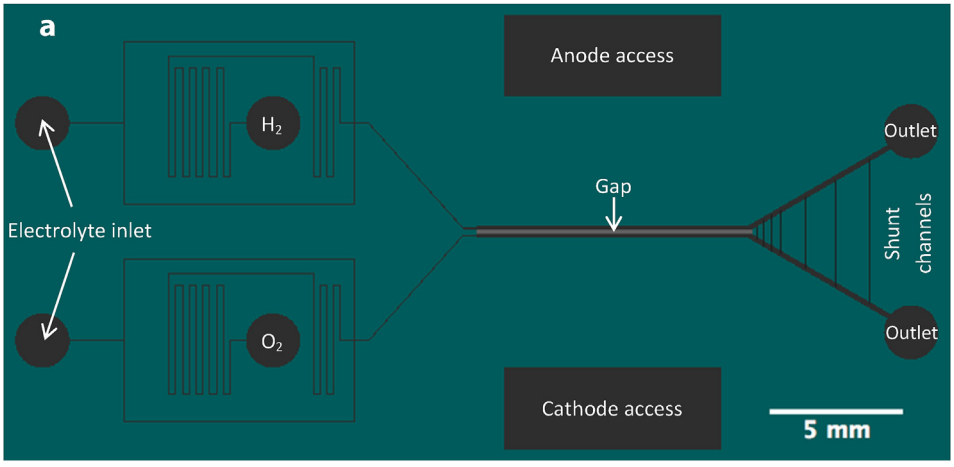

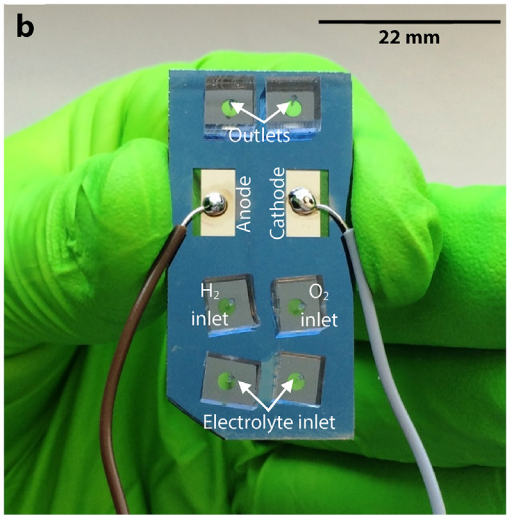

Fig. 3. a) Top view of the fluidic microchannels layout in a micro fuel cell. b) Photograph of a representative MFFC. PDMS pieces provide a flexible bed for introduction of electrolyte, fuel and oxidant streams. Anode and cathode connections to the potentiostat are established through conductive wires soldered to the Pt electrodes.

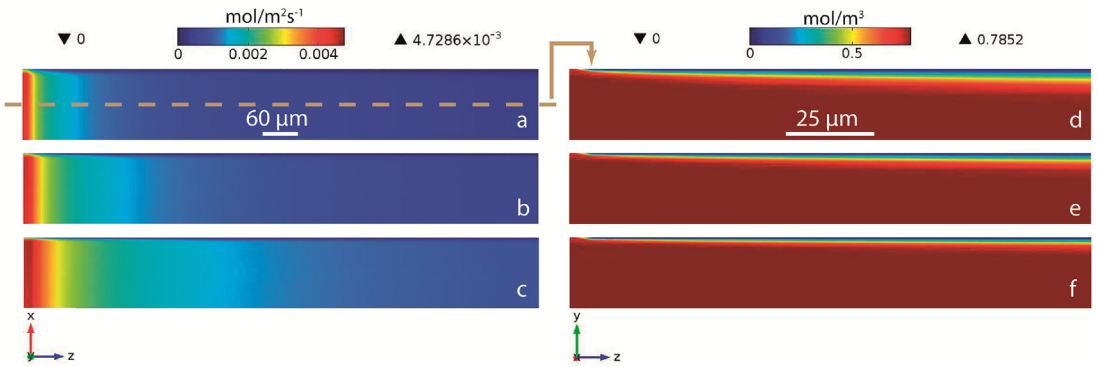

Fig. 4. Mass flux maps over the initial electrode area for fuel/oxidant flow rates of (a) 4 ml h^{-1}, (b) 8 ml h^{-1}, and (c) 16 ml h^{-1}. The concentration boundary layers formed right beneath the electrode in a plane passing through its middle are provided for the same flow rates on the right (d to f).

devices is visualized using an optical microscope in reflection mode. A fast camera (Photron's FASTCAM Mini UX100) is used for capturing videos at high frequencies.

The electrochemical characterization is performed using a VSP-300 Biologic Potentiostat. The measurements are done at three different flow rates for both single phase and two-phase cases. In order to have a fair comparison, the total flow rate for the two gases in the two-phase system is set equal to the total flow rate for the liquid electrolyte in the single phase case. In the two-phase case, the liquid electrolyte's flow rate is kept constant at the small value of 1 ml h^{-1} to provide ion conduction between the two electrodes. Unlike the single phase case, this stream is not saturated with any of the gases before flowing into the chip.

5. Results and discussion

As explained above, the main purpose of this study is to mitigate the mass transport limitations in MFFCs, which arise from the low solubility of hydrogen and oxygen in liquid electrolytes. In order to achieve this, a two-phase flow MFFC with two annular flows of each gas, i.e. H_2 and O_2, in a liquid electrolyte was developed. Under this configuration, mass transport models suggest that the maximum power density can be enhanced by up to a factor of 11 for a fuel/oxidant flow rate of 16 ml h^{-1}, when going from single phase to two-phase operation. To provide insights on the mass transport limitations for a one phase device, the mass flux maps together with the concentration boundary layers over the electrode are depicted in Fig. 4. Furthermore, the average values of flux are reported in Table 1 for comparison with the analytical values obtained for the two-phase case. Fig. 4a–c shows that the mass flux is highly non-uniform when we move along the electrodes and drops quite rapidly in the first few hundreds of microns. This clearly demonstrates that the single phase device suffers significantly from the lack of reactants at the vicinity of the electrode's surface, and the average mass flux drops drastically as a function of electrode distance (Fig. 4d–f). This is in contrast with the two-phase case where the mass flux is expected to remain approximately uniform throughout the length of the electrode, making the two-phase device intrinsically scalable. It must be noted however that as the gases get consumed, the water generated over the cathode surface will enter the liquid phase, the thickness of the film will vary and the conductivity of the electrolyte is expected to decrease. Under the operating conditions tested in this study, these effects did not affect noticeably the operation of the devices.

To experimentally demonstrate the potential of the proposed MFFC architecture, devices were fabricated and characterized under various operating conditions. The top view of the device during operation is shown in Fig. 5, both at the inlet and outlet of the cell. These images show that the elongated bubbles are confined to their corresponding channels and do not enter the narrow gap in between. This is due to the fact that entering this region will increase the surface energy of the gas bubbles and, therefore, is thermodynamically unfavorable. Movies S1 and S2 show clearly this phenomenon. Fig. 5 and the supporting videos demonstrate that the flow inside the channels is approaching an annular profile. Within this flow profile, gas transport towards the electrodes can be enhanced as molecules only need to diffuse through a thin layer of electrolyte covering the electrodes; at the same time the ionic

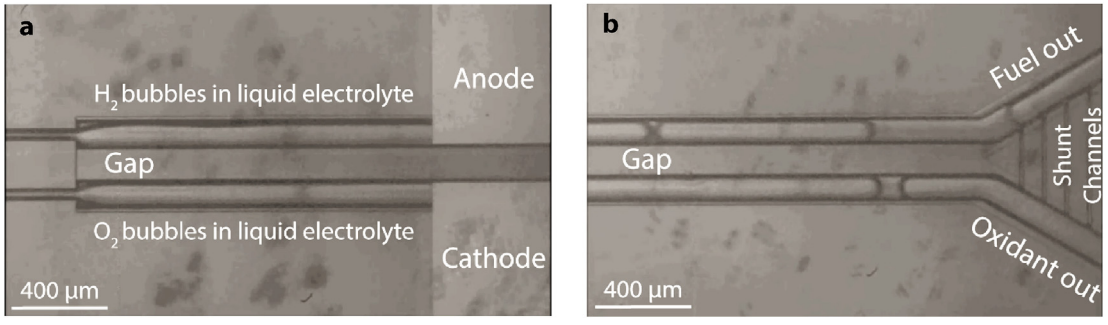

Fig. 5. Top view of the device during operation under a total 16 ml h^{-1} gas flow (8 ml h^{-1} for each gas stream) and 1 ml h^{-1} of electrolyte flow: (a) beginning of the cell, and (b) end of the cell. Thermodynamically, the gases minimize their surface energy by being confined to each of the channels above the electrodes and do not enter the shallow gap in between. The electrolyte fills in the gap and surrounds the gases, providing ionic conduction between the anode and cathode. Shunt channels in (b) provide pressure balance between the two outlet branches and prevent any potential bubble clogging.

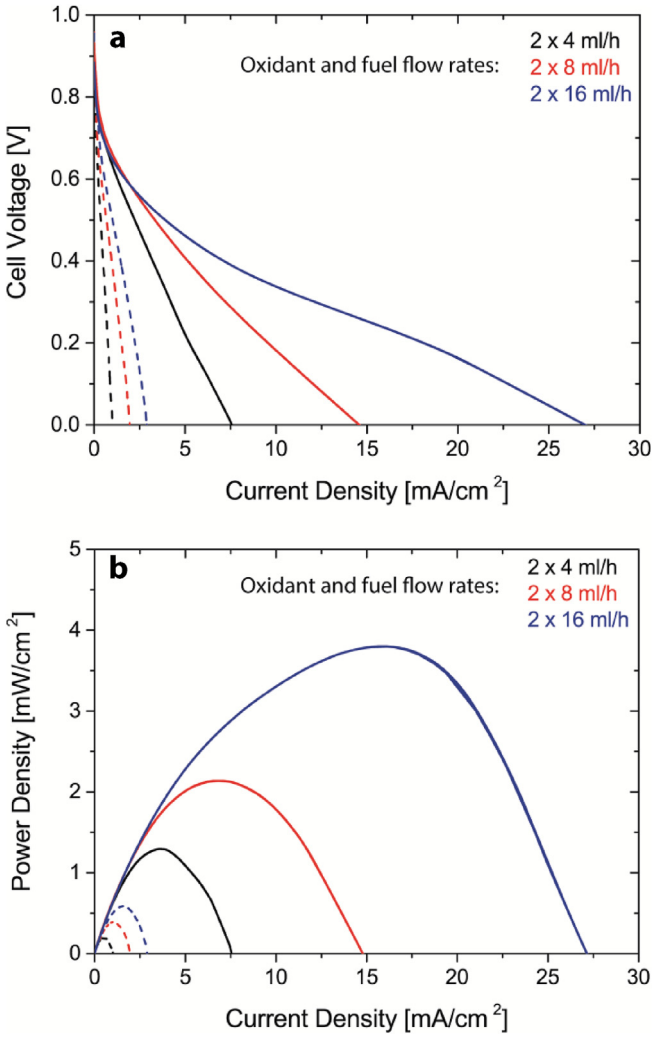

Fig. 6. (a) Polarization and (b) power density profiles of all devices at three different flow rates. Solid lines and dashed lines correspond to the two-phase and single phase device respectively. Higher power densities are demonstrated for the two-phase device, suggesting an increased mass-transfer of gases to the electrodes. Expanded plots for the single phase devices are provided in SI.

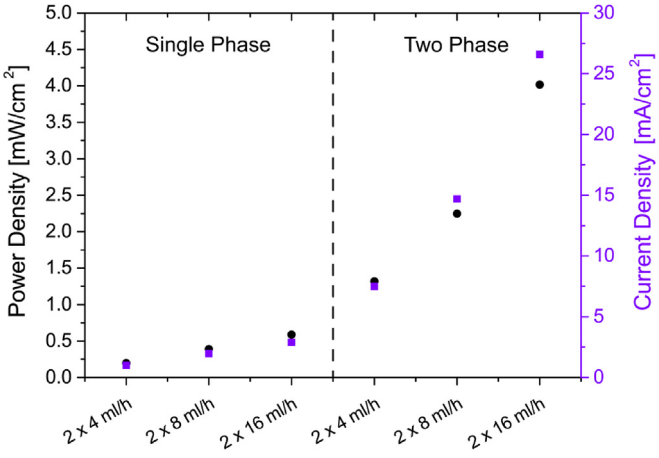

Fig. 7. Comparison of peak power densities and short circuit currents at different flow rates under single and two-phase configurations.

resistance can be high, as ions are restricted to migrate through this thin film of electrolyte. The potentiostatic electrochemical impedance spectroscopy (PEIS) measurements show only a ~28 Ω difference between the resistivity of the two device configurations. This is likely caused by the in-plane electrode architecture of the cells where most of the current is expected to pass through the inner edges of the electrodes, and the ionic conductivity of the device is defined by the shallow gap connecting the two channels. Since this gap is the same for both the single and two-phase cases, the conductivity values are not expected to differ significantly. The negligible difference between the cells resistivity, ~3 Ω, operating at different gas flow rates in the two-phase case is another indication that most of the current passes through the electrodes closest edges. At larger gas flow rates, the electrolyte film thickness is smaller and, therefore, the ionic conductivity is expected to be smaller. At low currents and overpotentials, the reaction is expected to take place mostly at the inner edges of the electrodes because the losses will be dominated by the electrolyte resistance. As the current increases, its distribution over the surface of electrodes becomes more uniform since the overpotential losses increase and become comparable to the ohmic losses. These asymmetries in the current density distribution would lead to an ionic resistance that is highly dependent on the overall operating current.

Fig. 5b also shows that a significant portion of reactants exit the device without participating in the reaction. This low fuel consumption per cycle is a shortcoming for all MFFCs, but the advantage in our two-phase system is that the fuel recycling can be done in a practical way. In the single phase MFFCs, the area around the streams interface at the end of the channel contains both fuel and oxidant, making it difficult to separate them precisely and reintroduce them into the device. On the contrary, it can be seen from Fig. 5b and Movie S2 that this separation is actively done in the present device and, therefore, recycling in this device is possible. A potential way of maximizing the fuel and oxidant utilization and, therefore, minimizing the need for recycling is to make an array of the cells on a wafer and allowing for fluidic and electronic communication between them. This method also generates a higher voltage and/or current, depending on the way the cells are interfaced with each other. The challenge in doing so lies at connecting these cells in a planar configuration. Several architectures for series and parallel interconnections in a planar stack could be employed for scale out of the present MFFC [29–31].

The polarization and power density curves of the fuel cell are provided in Fig. 6a and Fig. 6b, respectively. Open circuit voltages are all close to 1 V, suggesting that the fuel crossover in all cases is similar and negligible. Detailed results for the single phase case are provided in Fig. S3 and correlate well with values obtained elsewhere [16]. The current and power densities of the two-phase case are one order of magnitude higher than that for the single phase, suggesting that mass transport limitations have been alleviated by the introduction of controlled two-phase streams.

Fig. 7 compares the peak power density and short circuit current density values for the two-phase and single phase cases at all the flow rates tested. The experimental values are comparable with those obtained from the mass transport model described in Section 3, indicating that mass transport losses limit the performance of these fuel cell devices.

Table 1 summarizes the average flux values, their ratios, and the ratio between the short circuit currents at each flow rate for both single phase and two-phase conditions. It can be seen that for higher flow rates, the simulation data overpredict the enhancement, suggesting that other limiting processes start to play a significant role.

Table 1
Average flux value ratios from modeling and comparison with short circuit current ratios from experiment.

Flow rate [ml hr^{-1}]	Two-phase			Single phase		Average flux ratios (modeling)	$\frac{J_{sc}^{2phase}}{J_{sc}^{1phase}}$ (experimental)
	d [μm]	Average flux [mol m^{-2} s^{-1}]	J_{sc} [mA cm^{-2}] (Fig. 7)	Average flux [mol m^{-2} s^{-1}]	J_{sc} [mA cm^{-2}] (Fig. 7)		
4	2.02	1.74×10^{-3}	7.5	2.94×10^{-4}	1	5.9	7.5
8	1.06	3.31×10^{-3}	14.7	4.19×10^{-4}	1.96	7.9	7.5
16	0.54	6.50×10^{-3}	26.6	5.89×10^{-4}	2.9	11	9.2

6. Conclusion

This study demonstrates that the mass transport limitations of single phase MFFCs operating with hydrogen and oxygen saturated electrolytes can be relaxed by introducing H_2 and O_2 annular flows in electrolytes. By allowing gas streams to minimize their surface energy in confined microfluidic channels, we demonstrate that gas mixing can be prevented. The results show that the two-phase system delivers one order of magnitude better performance compared to its single phase counterpart. The method introduced here, opens up a pathway to revisit the utilization of gaseous hydrogen in high power density MFFCs which was hindered by its low solubility in liquid electrolytes. Such a technique can be used in other electrochemical systems to boost their performance by relaxing potential mass transfer limitations. The power densities obtained in this work can be further improved by optimizing dimensions such as the gap size and using micro/nanostructured electrodes. These electrodes induce mixing in the concentration boundary layer while providing higher active area for reactions to take place.

Acknowledgments

The work was funded by the grant no. 20NA21-145936 of Nano-Tera Initiative for Solar Hydrogen Integrated Nano Electrolyzer (SHINE) project. The authors would like to thank Professor Christophe Moser and Professor Sophia Hasussener's groups for providing access to their laboratory equipment, and Professor Elise Lorenceau for fruitful discussions.

Appendix A. Supplementary data

Supplementary data related to this article can be found at http://dx.doi.org/10.1016/j.jpowsour.2017.02.079.

References

[1] J.M. Andujar, F. Segura, Fuel cells: history and updating. A walk along two centuries, Renew. Sustain. Energy Rev. 13 (9) (2009) 2309–2322.
[2] M.E. Oruc, et al., Design, fabrication, and characterization of a proposed microchannel water electrolyzer, J. Power Sources 307 (2016) 122–128.
[3] A. Simons, C. Bauer, A life-cycle perspective on automotive fuel cells, Appl. Energy 157 (2015) 884–896.
[4] T.S. Zhao, Micro Fuel Cells : Principles and Applications, Academic Press, Amsterdam, Boston, 2009 ix, 300 p.
[5] J.D. Morse, Micro-fuel cell power sources, Int. J. Energy Res. 31 (6–7) (2007) 576–602.
[6] M.A. Modestino, et al., The potential for microfluidics in electrochemical energy systems, Energy Environ. Sci. 9 (11) (2016) 3381–3391.
[7] H. Ren, H.S. Lee, J. Chae, Miniaturizing microbial fuel cells for potential portable power sources: promises and challenges, Microfluid. Nanofluid. 13 (3) (2012) 353–381.
[8] H.Y. Wang, et al., Micro-sized microbial fuel cell: a mini-review, Bioresour. Technol. 102 (1) (2011) 235–243.
[9] D.S. Falcao, et al., Review on micro-direct methanol fuel cells, Renew. Sustain. Energy Rev. 34 (2014) 58–70.
[10] M.A. Goulet, E. Kjeang, Co-laminar flow cells for electrochemical energy conversion, J. Power Sources 260 (2014) 186–196.
[11] E. Kjeang, N. Djilali, D. Sinton, Microfluidic fuel cells: a review, J. Power Sources 186 (2) (2009) 353–369.
[12] M.N. Nasharudin, et al., Mass transfer and performance of membrane-less micro fuel cell: a review, Int. J. Hydrogen Energy 39 (2) (2014) 1039–1055.
[13] S.A.M. Shaegh, N.T. Nguyen, S.H. Chan, A review on membraneless laminar flow-based fuel cells, Int. J. Hydrogen Energy 36 (9) (2011) 5675–5694.
[14] M. Safdar, J. Janis, S. Sanchez, Microfluidic fuel cells for energy generation, Lab a Chip 16 (15) (2016) 2754–2758.
[15] J.L. Cohen, et al., A dual electrolyte H-2/O-2 planar membraneless microchannel fuel cell system with open circuit potentials in excess of 1.4 V, Langmuir 21 (8) (2005) 3544–3550.
[16] J.L. Cohen, et al., Fabrication and preliminary testing of a planar membraneless microchannel fuel cell, J. Power Sources 139 (1–2) (2005) 96–105.
[17] E. Kjeang, et al., A microfluidic fuel cell with flow-through porous electrodes, J. Am. Chem. Soc. 130 (12) (2008) 4000–4006.
[18] J.W. Lee, M.A. Goulet, E. Kjeang, Microfluidic redox battery, Lab a Chip 13 (13) (2013) 2504–2507.
[19] N.D. Mota, et al., Membraneless, room-temperature, direct borohydride/cerium fuel cell with power density of over 0.25 W/cm^2, J. Am. Chem. Soc. 134 (14) (2012) 6076–6079.
[20] S.M.H. Hashemi, M.A. Modestino, D. Psaltis, A membrane-less electrolyzer for hydrogen production across the pH scale, Energy & Environmental Science 8 (7) (2015) 2003–2009.
[21] P. Abbyad, et al., Rails and anchors: guiding and trapping droplet microreactors in two dimensions, Lab a Chip 11 (5) (2011) 813–821.
[22] E. Fradet, et al., Combining rails and anchors with laser forcing for selective manipulation within 2D droplet arrays, Lab a Chip 11 (24) (2011) 4228–4234.
[23] M. Nagel, P.T. Brun, F. Gallaire, A numerical study of droplet trapping in microfluidic devices, Phys. Fluids 26 (3) (2014).
[24] R. Dangla, S. Lee, C.N. Baroud, Trapping microfluidic drops in wells of surface energy, Phys. Rev. Lett. 107 (12) (2011).
[25] P. Gruner, et al., Controlling molecular transport in minimal emulsions, Nat. Commun. 7 (2016).
[26] P.O. Lopez-Montesinos, et al., Design, fabrication, and characterization of a planar, silicon-based, monolithically integrated micro laminar flow fuel cell with a bridge-shaped microchannel cross-section, J. Power Sources 196 (10) (2011) 4638–4645.
[27] M.J. Fuerstman, et al., The pressure drop along rectangular microchannels containing bubbles, Lab a Chip 7 (11) (2007) 1479–1489.
[28] A.R. Abate, J.J. Agresti, D.A. Weitz, Microfluidic sorting with high-speed single-layer membrane valves, Appl. Phys. Lett. 96 (20) (2010).
[29] S.J. Lee, et al., Design and fabrication of a micro fuel cell array with "flip-flop" interconnection, J. Power Sources 112 (2) (2002) 410–418.
[30] H.Z. Wang, et al., Development and characteristics of a membraneless microfluidic fuel cell array, Electrochim. Acta 135 (2014) 467–477.
[31] H.J. Hou, et al., A microfluidic microbial fuel cell array that supports long-term multiplexed analyses of electricigens, Lab a Chip 12 (20) (2012) 4151–4159.